THE ASTROPHYSICAL JOURNAL, 200:6–21, 1975 August 15

OBSERVATIONS OF QUASI-THERMAL AND MASER PHENOMENA IN ROTATIONALLY EXCITED OH. I.

L. J RICKARD
University of Chicago
B. ZUCKERMAN*
University of California, Berkeley; and University of Maryland, College Park
AND
P. PALMER
University of Chicago
Received 1974 November 7

ABSTRACT

Absorption features arising from Λ-doublet transitions in a very short-lived rotationally excited state of OH have been discovered in the direction of the W3 continuum peak. Analyses of these features and of broad emission features in Sgr B2 indicate the presence of massive regions with very high densities. An extensive search for new sources of maser emission from excited-state OH has resulted in the detection of maser features in NGC 7538, OH 69.5−1.0, M17, W51, and Orion (OH). Observations with circular polarization suggest Zeeman effects in some spectra, with inferred magnetic field strengths of several milligauss. A rapid time variation has been observed in the maser spectrum of Sgr B2, and evidence is presented for variations in W51 and W3 (continuum).

Subject headings: infrared sources — masers — molecules, interstellar

I. INTRODUCTION

The first detection of emission from rotationally excited OH was that of the 6-cm Λ-doublet transition of the $^2\Pi_{1/2}$, $J = 1/2$ state (Zuckerman *et al.* 1968). Subsequently, similar emission features were observed at 5 and 2.2 cm, arising from the $^2\Pi_{3/2}$, $J = 5/2$ and $J = 7/2$ states (Yen *et al.* 1969; Turner, Palmer, and Zuckerman 1970). In all cases, the features are almost certainly maser emission (e.g., Knowles *et al.* 1973) and should help to clarify the mechanism responsible for the associated ground-state maser phenomena. These maser features, as well as those from H_2O, originate from very small regions (of solar system dimensions).

The subsequent detection of weak, broad (~20 km s^{-1} wide) emission features in the 6-cm OH spectra of the galactic center source Sgr B2 (Gardner, Ribes, and Sinclair 1971; Gardner and Ribes 1971) suggested that nonmaser emission is also observable from these excited states. We have searched for and detected similar 5-cm OH emission from the Sgr B2 source. Because of the very short lifetimes (~8 s) of the OH rotational levels, the nonmaser emission very probably originates from dense neutral regions (see discussion below) in the vicinity of H II regions and infrared sources. These neutral regions are probably the cores of the extended molecular clouds observed at millimeter wavelengths.

The formation of these broad, spatially extended, low surface brightness features is probably much more closely related to that of the millimeter-wavelength lines of such molecules as HCN, HC_3N, and CH_3CN (which require high densities to significantly populate the relevant energy levels) than to that of the OH maser lines. We have called these nonmaser OH features quasi-thermal (QT) to distinguish them from the maser features, and we will discuss the two types separately. The QT features differ from the maser features because (1) they come from a larger region and consequently have much lower brightness temperatures, (2) their velocity widths are much greater, (3) the relative intensities of their hyperfine components are usually similar to the local thermodynamic equilibrium (LTE) values, and (4) their velocity structure is usually simple, with the central velocity correlated with that of many millimeter-wavelength lines. The first criterion is the most definitive; but size information exists in only a few cases so far, usually necessitating the use of criteria 2–4 to distinguish QT features.

We have detected absorption features in both $\Delta F = 0$ hyperfine transitions at 5 cm against the W3 continuum source (Rickard, Zuckerman, and Palmer 1973). We believe that the $^2\Pi_{3/2}$, $J = 5/2$ state of OH is the shortest-lived state to be observed in absorption in the interstellar medium at any wavelength.

We have also detected some new maser emission sources, one at 6 cm (Ori A) and three at 5 cm (NGC 7538, OH 69.5−1.0,[1] M17), and are presenting observations of a fourth 5-cm maser source (W51) which was detected in 1971 (Gottlieb and Palmer,

* Alfred P. Sloan Foundation Research Fellow.

[1] This source has also been referred to as OH 2008+31 (e.g., Hardebeck 1972). We prefer to reference the source by its galactic coordinates.

private communication). Preliminary results for some of these observations have been reported elsewhere (Rickard, Zuckerman, and Palmer 1972, 1973). We have studied the circular polarization of the 5-cm spectra of W49, W51, NGC 7538, and OH 69.5−1.0; and we have observed time variations in some sources.

The present paper describes observations made at the National Radio Astronomy Observatory.[2] A subsequent paper will present observations made with the 100-meter antenna of the Max-Planck-Institut, at Effelsberg, West Germany. In the following sections, we briefly describe our equipment, and then describe our data and discuss the results in terms of the physical conditions within QT sources and the various pumping models proposed for the maser sources.

II. OBSERVATIONS

a) Equipment

We used the NRAO 140-foot (43 m) telescope and the 384-channel autocorrelation receiver. The 5-cm observations were made using an uncooled parametric amplifier, and the 6-cm observations were made with a cooled parameter amplifier. A summary of the observing sessions is given in Table 1. All observations were made in the total power mode, one off-source spectrum being subtracted from a number of on-source spectra shifted by 0, ±2, ±4, etc., channels. The temperature scales of the linearly polarized 5-cm spectra were calibrated by assuming a peak flux density of 57 Jy for Virgo A and an aperture efficiency of 49 percent. For the 6-cm spectra, we used a peak flux density of 69.6 Jy for Virgo A and an aperture efficiency of 50 percent.

b) Spectra of Individual Sources

The spectra of the newly detected lines are displayed in Figures 1–10. Observational results are given in Table 2 for all sources searched for QT features, and in Table 3 for all sources which showed maser features.

[2] The National Radio Astronomy Observatory is operated by Associated Universities, Inc., under contract with the National Science Foundation.

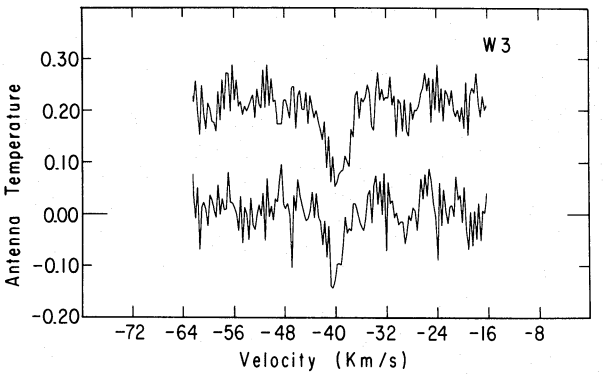

FIG. 1.—The $^2\Pi_{3/2}$, $J = 5/2$, $F = 3 \rightarrow 3$ and $F = 2 \rightarrow 2$ transitions in W3(cont). *Ordinate*, antenna temperature; *abscissa*, radial velocity with respect to the local standard of rest. The frequency resolution is 8 kHz. The $F = 3 \rightarrow 3$ transition has been shifted up by 0.2 K.

The parameters of the circular polarization measurements are given in Table 4. The results of the polarization observations are given in Table 5. The percentage of circular polarization is defined by $P = 100(T_{max} - T_{min})/(T_{max} + T_{min})$ and is given for the clearest features in the spectra. The sense of polarization is indicated by R, for right-circular, or L, for left-circular, where right-circular polarization is defined by clockwise rotation of the E-vector as seen by an observer looking along the direction of propagation. The listed errors are 1 σ errors determined from the single-channel rms deviations. When the errors include a negative percent of polarization (implying the opposite sense of polarization), the listed sense of polarization is enclosed in parentheses. Negative results for sources searched for 5-cm maser emission are given in Table 6, and for sources searched for 6-cm maser emission in Table 7.

i) *W3(continuum)*

In Figure 1, we display the spectra for the $^2\Pi_{3/2}$, $J = 5/2$, $F = 3 \rightarrow 3$ and $F = 2 \rightarrow 2$ transitions.[3] The

[3] In this article, we use the convention of labeling transitions $F \rightarrow F'$, where F refers to the total angular momentum of the upper state, and F' to that of the lower state.

TABLE 1

OBSERVATIONAL PARAMETERS

OBSERVING PERIOD	FHPB* α	FHPB* δ	POLARIZATION	T_{sys}† (K)
5-cm observations:	5′.2	5′.1		
1972 March			Linear	230
1972 November/December			Linear	205
1973 August			Right Circular	260
			Left Circular	260
			Linear	260
6.3-cm observations:	6′.8	6′.6		
1972 January			Linear	70
1973 July			Linear	70
1973 August			Linear	70

* Full half-power beamwidth.

† System temperature when looking at cold sky.

1975ApJ...200....6R

TABLE 2

SUMMARY OF SOURCES SEARCHED FOR QUASI-THERMAL FEATURES

Source	α_{1950}	δ_{1950}	Transition	Spectral Resolution (kHz)	Radial-Velocity Range Covered (km s^{-1})	T_A (K)	V_{LSR}* (km s^{-1})	ΔV† (km s^{-1})	$T_{continuum}$‡ (K)	Notes
W3(cont)....	$2^h21^m55^s$	61°52′35″	3 → 2	8	−65.7, −13.7	< 0.05	...	...	12.6	2
			3 → 3	8	−63.9, −15.7	−0.15	−40	4.4	...	2
			2 → 2	8	−63.9, −15.7	−0.15	−40	3	...	2
			2 → 3	8	−66.0, −13.8	< 0.05	...	...	...	2
			1 → 0	8	−74.4, −8.5	< 0.02	...	...	13.8	3
			1 → 1	8	−74.6, −8.4	< 0.02	...	...	...	3
			0 → 1	8	−73.1, −10.7	< 0.02	...	...	...	3
Virgo A.....	12 28 19	12 41 16	3 → 2	8	−32.8, +19.1	< 0.10	...	...	14.5	2
			3 → 3	8	−33.2, +18.9	< 0.08	...	...	...	2
			2 → 2	8	−33.2, +18.9	< 0.10	...	...	...	2
			2 → 3	8	−32.8, +19.1	< 0.08	...	...	...	2
			1 → 0	16	−29.9, +102.0	< 0.04	...	...	17.9	3
			1 → 1	16	−29.8, +102.5	< 0.03	...	...	...	3
			0 → 1	32	−90.1, +159.6	< 0.03	...	...	...	3
Sgr A.....	17 42 28	−28 58 30	1 → 0	63	−225.4, +302.1	< 0.05	...	...	...	1
			1 → 1	63	−226.2, +303.0	< 0.05	...	...	...	1
			0 → 1	16	−107.0, +188.7	< 0.07	...	...	...	1
Sgr B2.....	17 44 11	−28 22 30	3 → 2	32	−41.3, +166.5	< 0.02	...	...	9.0	2
			3 → 3	32	−41.4, +166.9	< 0.03	...	...	...	2, 4
			2 → 2	32	−41.4, +166.9	0.05	+60	20	...	2
			2 → 3	32	−41.6, +167.4	< 0.03	...	...	...	2
			1 → 0	16	−4.2, +127.7	0.04	+60	25	11.4	3
			1 → 1	16	−4.0, +128.3	0.09	+60	23	...	3
			0 → 1	32	−64.8, +184.8	0.15	+60	18	...	3
Cloud 12....	17 44 21	−28 14 08	0 → 1	16	−103.5, +186.6	< 0.02	...	...	...	1
Cloud 13....	17 44 59	−28 12 08	1 → 0	32	−94.9, +168.9	< 0.04	...	...	...	1
			1 → 1	32	−95.3, +169.3	< 0.04	...	...	...	1
			0 → 1	16	−92.8, +197.2	< 0.04	...	...	...	1
Cloud 15....	17 46 28	−27 28 01	1 → 0	32	−95.1, +169.5	< 0.04	...	...	...	1
			1 → 1	32	−94.7, +169.1	< 0.04	...	...	...	1
			0 → 1	32	−82.7, +186.8	< 0.05	...	...	...	1
M17.....	18 17 36	−16 12 17	1 → 0	63	−225.8, +301.7	< 0.02	...	...	...	1
			1 → 1	63	−226.6, +302.6	< 0.10	...	...	...	1

* Radial velocity with respect to the local standard of rest.

† Full line width at half-maximum intensity.

‡ Continuum antenna temperature, given for all transition frequencies within each rotational state. Values are given for the two detected sources and, for comparison for Virgo A.

NOTES.—(1) Observed in 1972 January. (2) Observed in 1972 November/December. (3) Observed in 1973 July. (4) Spectrum dominated by strong maser features in the region 60 km s^{-1} ≤ v_{LSR} ≤ 75 km s^{-1}. Upper limit refers to velocities outside this region.

TABLE 3

OBSERVATIONAL RESULTS FOR SOURCES WITH MASER EMISSION

Source	α_{1950}	δ_{1950}	Transition	Spectral Resolution (kHz)	Radial-Velocity Range Covered (km s^{-1})	RMS Noise (K)	Note
W3(cont).....	$2^h21^m55^s$	61°52′35″	3 → 2	8	−65.7, −13.7	0.117	3, 6
			3 → 3	8	−63.9, −15.7	0.049	3, 6
			2 → 2	8	−63.9, −15.7	0.046	3, 6
			2 → 3	8	−66.0, −13.8	0.060	3, 6
			1 → 0	8	−74.4, −8.5	0.010	4
			1 → 0	1	−37.9, −31.5	0.240	4
			1 → 1	8	−74.6, −8.4	0.009	4, 6
			0 → 1	8	−73.1, −10.7	0.012	4, 6
W3 (OH).....	2 23 17	61 39 00	3 → 3	2	−50.2, −37.2	0.212	3
			2 → 2	2	−50.2, −37.2	0.200	3
			1 → 0	1	−49.0, −40.8	0.170	1
			1 → 1	8	−78.3, −12.1	0.029	1, 6
Orion (OH).....	5 32 47	− 5 24 20	3 → 2	8	−16.2, +35.8	0.059	2, 6
			3 → 3	8	−16.3, +35.8	0.059	2, 6
			2 → 2	8	−16.3, +35.8	0.060	2, 6
			2 → 3	8	−16.0, +36.2	0.054	2, 6
			0 → 1	4	−31.7, +48.8	0.045	1
			0 → 1	1	−1.5, +18.6	0.138	1
NGC 6334 N.....	17 17 32	−35 44 20	3 → 3	2	−13.2, −0.2	0.136	3
			2 → 2	2	−13.2, −0.2	0.106	3
Sgr B2.....	17 44 11	−28 22 30	3 → 2	32	−41.3, +166.5	0.031	3, 6
			3 → 3	32	−41.4, +166.9	0.096	3
			2 → 2	32	−41.4, +166.9	0.058	3, 6
			2 → 3	32	−41.6, +167.4	0.037	3, 6
			1 → 0	32	−70.5, +193.3	0.014	4
			1 → 1	32	−70.6, +194.0	0.008	4, 6
			0 → 1	32	−64.8, +184.8	0.037	4
			0 → 1	2	+48.6, +64.2	0.042	4
M17.....	18 17 29	−16 13 42	3 → 3	8	−1.8, +50.3	0.090	5
			3 → 3	2	+17.8, +30.8	0.108	5
			2 → 2	8	−1.8, +50.3	0.094	5
			2 → 2	2	+17.8, +30.8	0.100	5
			1 → 0	8	−8.8, +57.1	0.069	4, 6
			1 → 1	8	−8.8, +57.4	0.076	4, 6
			0 → 1	8	+4.3, +66.7	0.052	4, 6
W49.....	19 07 53	9 01 00	3 → 3	4	+0.2, +26.3	0.085	3
			2 → 2	4	+0.2, +26.3	0.090	3, 6
W51.....	19 21 27	14 24 30	3 → 3	8	+31.2, +83.2	0.055	3
			3 → 3	2	+50.8, +63.9	0.130	3
			2 → 2	8	+31.2, +83.2	0.069	3
			2 → 2	2	+50.8, +63.9	0.134	3
			1 → 0	4	+43.1, +76.1	0.082	1, 6
			1 → 1	8	+26.2, +92.7	0.057	1, 6
			0 → 1	4	+22.8, +96.7	0.036	1, 6
OH 69.5−1.0.....	20 08 10	31 22 41	3 → 3	8	−10.4, +41.7	0.055	3
			3 → 3	2	+9.3, +22.3	0.085	3
			2 → 2	8	−10.4, +41.7	0.055	3, 6
			2 → 2	2	+9.3, +22.3	0.091	3, 6
			0 → 1	8	−19.1, +48.3	0.028	5, 6
W75 N.....	20 36 50	42 26 58	3 → 3	2	+1.8, +14.8	0.195	3
			2 → 2	2	+1.8, +14.8	0.153	3, 6
NGC 7538.....	23 11 37	61 11 48	3 → 3	2	−64.2, −51.2	0.099	3
			2 → 2	2	−64.2, −51.2	0.095	3, 6
			1 → 0	4	−75.5, −42.6	0.047	4, 6
			1 → 1	4	−75.7, −42.6	0.040	4, 6
			0 → 1	8	−92.8, −25.4	0.018	5, 6

NOTES.—(1) Observed in 1972 January. (2) Observed in 1972 March. (3) Observed in 1972 November/December. (4) Observed in 1973 July. (5) Observed in 1973 August. (6) No maser emission feature detected.

ratio of equivalent widths is consistent with the optically thin LTE ratio of $(3 \rightarrow 3)/(2 \rightarrow 2) = 20/14$. From considerations of beam filling (see § III*a*), we can be confident that these features originate from a much larger region than the maser emission features observed in this and other sources.

We searched for features at the frequencies of the $\Delta F = 1$ transitions, but obtained only upper limits (Table 2) which correspond to equivalent widths more than 6 times those expected from optically thin LTE relative intensities. The velocities and line widths of the $\Delta F = 0$ features agree with those of the 1665- and 1667-MHz absorption features in W3 (Turner 1970). The equivalent widths of these ground-state features

TABLE 4

OBSERVATIONAL PARAMETERS FOR POLARIZATION MEASUREMENTS

Source	Transition	Spectral Resolution (kHz)	Polarization	Radial-Velocity Range Covered (km s^{-1})	RMS Noise (K)
W3 (OH).....	3 → 3	2	L	−51.6, −38.6	0.581
			R	−51.6, −38.7	0.472
	2 → 2	2	L	−51.6, −38.7	0.412
			R	−51.6, −38.7	0.457
Sgr B2.....	3 → 3	4	L	+49.3, +75.3	0.118
			R	+49.3, +75.3	0.109
W49.....	3 → 3	2	L	+5.9, +18.9	0.117
			R	+5.9, +18.9	0.132
W51.....	3 → 3	2	L	+47.9, +60.9	0.118
			R	+47.9, +60.9	0.135
	2 → 2	2	L	+47.9, +60.9	0.128
			R	+47.9, +60.9	0.119
OH 69.5−1.0.....	3 → 3	2	L	+8.3, +21.3	0.182
			R	+8.3, +21.3	0.129
NGC 7538.....	3 → 3	2	L	−65.3, −53.2	0.163
			R	−65.5, −53.5	0.127

TABLE 5

POLARIZATION MEASUREMENTS

Feature	Radial Velocity (km s^{-1})	Polarization (percent)	Sense of Polarization
	W51, 3 → 3		
1.....	53.05	46 ± 14	L
2.....	53.37	19 ± 8	R
3.....	53.53	8 ± 10	(L)
4.....	53.78	78 ± 18	R
5.....	54.75	0 ± 19	
6.....	54.91	37 ± 34	R
7.....	55.31	67 (+33, −68)	(L)
8.....	55.64	79 (+21, −35)	R
	W51, 2 → 2		
1.....	53.00	58 ± 30	L
2.....	53.32	39 ± 24	R
	NGC 7538, 3 → 3		
1.....	−59.76	1 ± 9	(L)
	OH 69.5−1.0, 3 → 3		
1.....	13.62	46 ± 15	R
2.....	13.79	13 ± 20	(L)
3.....	14.19	0 ± 5	
4.....	14.92	100 (+0, −33)	R
5.....	15.24	65 ± 34	L
	W49, 3 → 3		
1.....	9.93	68 (+32, −37)	R
2.....	10.18	41 ± 22	L
3.....	13.01	59 ± 25	R
4.....	15.51	3 ± 19	(R)

are in their optically thin LTE ratios, and these features must (from beam-filling arguments) originate in a source much larger than typical maser sources. Millimeter-wavelength emission from a number of molecules (such as H_2CO, CO, CS, HCN, and H_2S) is observed in this source at radial velocities near −40 km s^{-1}.

Since the presence of absorption features in this state was quite unexpected—the lifetime of the $^2\Pi_{3/2}$, $J = 5/2$ state against radiative decay to the ground

TABLE 6

NEGATIVE RESULTS FOR THE $^2\Pi_{3/2}$, $J = 5/2$ STATE MASER EMISSION

Source	α_{1950}	δ_{1950}	Transition	Spectral Resolution (kHz)	Radial-Velocity Range Covered (km s^{-1})	RMS Noise (K)	Note
L1521 #3	$4^h30^m26^s$	26°12′24″	3 → 3	8	−20.3, +31.8	0.104	3
			2 → 2	8	−20.3, +31.8	0.120	3
NGC 2024	5 39 12	− 1 55 40	3 → 3	4	−2.7, +23.3	0.070	2
			2 → 2	4	−2.7, +23.3	0.069	2
S247	6 05 40	21 36 00	3 → 3	8	−26.5, +25.5	0.125	3
			2 → 2	8	−26.6, +25.5	0.112	3
IC 2162	6 10 00	18 00 00	3 → 3	8	−26.6, +25.5	0.050	3, 4
			2 → 2	8	−26.6, +25.5	0.056	3, 4
S269	6 11 46	13 50 35	3 → 3	8	−26.5, +25.6	0.104	3, 5
			2 → 2	8	−26.5, +25.6	0.111	3, 5
NGC 2264	6 38 25	9 32 29	3 → 3	4	−5.6, +20.4	0.053	2
			2 → 2	4	−5.6, +20.4	0.056	2
VY CMa	7 20 53	−25 40 24	3 → 3	16	−31.0, +73.2	0.045	2
			2 → 2	16	−31.0, +73.2	0.049	2
OH 231.8+4.3	7 39 59	−14 36 11	3 → 3	16	−32.2, +72.0	0.051	2, 7
			2 → 2	16	−32.2, +72.0	0.055	2, 7
IRC+10216	9 46 26	13 24 40	3 → 3	8	−49.7, +2.4	0.042	3, 6
			2 → 2	8	−49.7, +2.4	0.045	3, 6
Cloud 4 (NH_3)	16 24 08	−24 28 00	3 → 3	8	−19.8, +32.3	0.066	2
			2 → 2	8	−19.8, +32.3	0.062	2
W28 A_2	17 57 27	−24 03 55	3 → 3	8	−50.9, +1.2	0.107	3
			2 → 2	8	−50.9, +1.2	0.089	3
W28 A_1	17 58 49	−23 18 32	3 → 3	8	−14.9, +37.2	0.075	2
			2 → 2	8	−14.9, +37.2	0.088	2
OH 10.6−0.4	18 07 27	−19 57 36	3 → 3	8	−26.3, +25.7	0.082	3
			2 → 2	8	−26.3, +25.8	0.081	3
W33 S	18 11 00	−18 02 47	3 → 3	8	+38.1, +90.2	0.069	3
			2 → 2	8	+38.2, +90.3	0.070	3
W33 N	18 11 42	−17 53 06	3 → 3	8	+14.2, +66.2	0.118	2
			2 → 2	8	+14.2, +66.2	0.125	2
W43 A	18 45 05	− 1 48 18	3 → 3	8	+15.7, +67.7	0.059	2
			2 → 2	8	+15.7, +67.7	0.069	2
OH 30.8−0.0	18 45 22	− 2 00 06	3 → 3	8	+84.2, +136.2	0.071	3
			2 → 2	8	+84.2, +136.3	0.080	3
OH 34.3+0.1	18 50 48	1 11 06	3 → 3	8	+37.2, +89.3	0.116	3
			2 → 2	8	+37.2, +89.3	0.111	3
W44	18 54 00	1 23 41	3 → 3	8	+19.7, +71.8	0.077	2
			2 → 2	8	+19.7, +71.8	0.080	2
OH 48.6+0.0	19 18 09	13 19 18	3 → 3	8	−5.8, +46.3	0.074	3
			2 → 2	8	−5.8, +46.3	0.081	3
OH 70.3+1.6	19 59 59	33 26 02	3 → 3	8	−37.9, +14.2	0.096	2
			2 → 2	8	−37.9, +14.2	0.089	2
OH 75.8+0.3	20 19 52	37 17 03	3 → 3	8	−22.4, +29.7	0.078	3
			2 → 2	8	−22.4, +29.7	0.070	3
DR 21 (OH)	20 37 14	42 12 00	3 → 3	8	−22.9, +29.2	0.074	3
			2 → 2	8	−22.9, +29.2	0.078	3
NML Cyg	20 44 40	39 55 46	3 → 3	8	−22.2, +29.8	0.106	1, 8
			2 → 2	8	−22.2, +29.8	0.102	1, 8

NOTES—(1) Observed in 1972 March. (2) Observed in 1972 Nobember/December. (3) Observed in 1973 August. (4) Average of equal amounts of left- and right-circular polarization data. (5) Observed with left-circular polarization only. (6) Average of linear polarization data with equal amounts of left- and right-circular polarization data. (7) Position is from Hardebeck (1972) and is probably 30″ S of true position (e.g., Wynn-Williams *et al.* 1974). (8) Pointing position was incorrect. True position is 1^s W, 6″N of this.

state is only ~8 s, and one might not expect such high excitation over a large enough region to produce detectable absorption—we made several variations in our observing technique to test the reality of the features. We varied the position at which the off-source spectrum was taken. We varied the frequency of the center of the bandpass for the off-source spectrum while holding it constant for the on-source spectra. We also varied the frequency of the bandpass center for both spectra together. In all cases, the absorption features behaved in the manner expected of real features. Finally, we observed Virgo A with all the various observing techniques, in order to search for a spurious feature. (The upper limits for Virgo A are given in Table 2.) Thus, the features are undoubtedly real.

During the 1973 August observing session, we attempted to determine the spatial distribution of the absorption features by making a four-point map around the continuum maximum. Because of the large

TABLE 7

NEGATIVE RESULTS FOR THE $^2\Pi_{1/2}$, $J = 1/2$ STATE MASER EMISSION

Source	α_{1950}	δ_{1950}	Transition	Spectral Resolution (kHz)	Radial-Velocity Range Covered (km s^{-1})	RMS Noise (K)	Note
IC 2162.....	$6^h10^m00^s$	18°00′00″	1 → 0	8	−33.8, +32.1	0.026	2
			1 → 1	8	−33.8, +32.4	0.022	2
S269.....	6 11 46	13 50 35	1 → 0	8	−35.2, +30.8	0.019	2
			1 → 1	8	−35.1, +31.0	0.020	2
NGC 2264.....	6 38 25	9 32 29	1 → 0	2	+1.7, +18.2	0.125	1
			1 → 1	8	−23.2, +43.0	0.051	1
			0 → 1	8	−28.3, +39.2	0.019	3
OH 231.8+4.3.....	7 39 59	−14 36 11	1 → 0	16	−48.2, +83.7	0.014	2
			1 → 1	16	−48.2, +84.1	0.014	2
IRC+10216.....	9 46 26	13 24 40	0 → 1	8	−57.0, +10.5	0.024	3
Cloud 4 (NH_3).....	16 24 08	−24 28 00	0 → 1	2	−16.7, +19.6	0.097	1
Cloud 15.....	17 46 28	−27 28 01	0 → 1	4	+35.8, +69.5	0.029	1
W28 A_2.....	17 57 27	−24 03 55	0 → 1	8	−58.6, +8.8	0.017	3
W33 S.....	18 11 00	−18 02 47	1 → 0	8	+31.0, +97.0	0.024	2
			1 → 1	8	+31.2, +97.4	0.021	2
OH 48.6+0.0.....	19 18 09	13 19 18	1 → 0	8	−13.3, +52.7	0.028	2
			1 → 1	8	−13.3, +52.9	0.026	2
OH 75.8+0.3.....	20 19 52	37 17 03	1 → 0	8	−29.5, +36.5	0.027	2
			1 → 1	8	−29.5, +36.6	0.025	2
			0 → 1	8	−30.1, +37.3	0.021	3
DR 21 (OH).....	20 37 14	42 12 00	0 → 1	4	−36.7, +35.8	0.022	1

NOTES.—(1) Observed in 1972 January. (2) Observed in 1973 July. (3) Observed in 1973 August.

beam size and the weakness of the features, we were only able to get an upper limit of 4′.7 to the angular extent of the cloud. However, by assuming a Gaussian source and Gaussian beam, we were also able to show that, while the features are strongest at the continuum peak, the line-to-continuum ratio (and thus, in a simple approximation, the optical depth) is peaked at $2^h21^m35^s$, 61°52′23″ (1950.0), about 2′.3 W of the continuum maximum.

In 1973 July, we searched for corresponding absorption features arising from the $^2\Pi_{1/2}$, $J = 1/2$ state. The only features found were two narrow ($\sim\frac{1}{2}$ km s^{-1}) emission features at 4765 MHz, shown in Figure 2. These maser lines are centered at −33.9, and −37.3 km s^{-1}. The weaker feature is in the usual velocity range for features in W3, but the only emission known at the velocity of the main feature is low-intensity H_2O emission (Sullivan 1971).

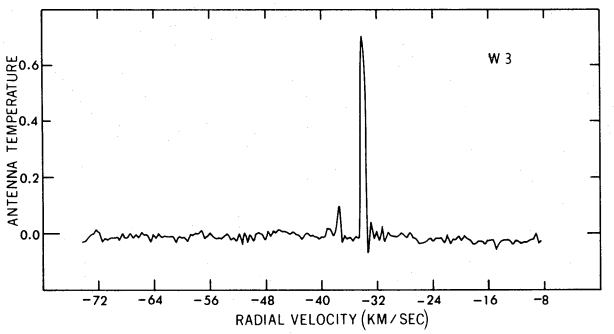

FIG. 2.—The $^2\Pi_{1/2}$, $J = 1/2$, $F = 1 \rightarrow 0$ transition in W3(cont). The frequency resolution is 8 kHz.

ii) *Sagittarius B2*

In Figure 3, we have displayed the spectrum for the $^2\Pi_{3/2}$, $J = 5/2$, $F = 2 \rightarrow 2$ transition, as observed in 1972 December. (The 1972 March observations of this source were rendered unusable because of the presence of a sinusoidal baseline ripple. When this problem recurred on the first day of the December observing run, it was identified as arising from reflections in a cable, and was corrected. The data from that first day were discarded.) The spectrum of the $F = 3 \rightarrow 3$ transition is dominated by maser emission features (see Fig. 11) which, at this resolution, would overwhelm thermal features as weak as the observed $F = 2 \rightarrow 2$ feature. The feature at 6031 MHz matches, in width and radial velocity, the broad features observed at 6 cm (Gardner and Ribes 1971). The ground-state OH spectra are rather complex, and there is no specific

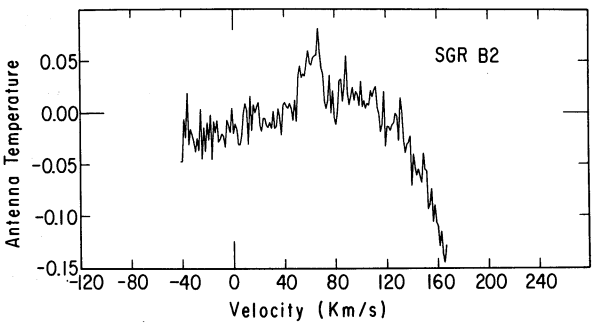

FIG. 3.—The $^2\Pi_{3/2}$, $J = 5/2$, $F = 2 \rightarrow 2$ transition in Sgr B2. The frequency resolution is 31.5 kHz. The baseline curvature at high velocities results from slow changes in the receiver bandpass shape which occur at this bandwidth.

feature with which we may associate the excited-state features, but the maximum depth of the absorption profile at 1667 MHz does fall at the same radial velocity (Palmer and Zuckerman 1967). This is also the velocity at which most of the molecules recently discovered in this source have been found.

We observed the broad features at 6 cm in 1973 July and obtained spectra essentially in agreement with those of Gardner and Ribes. Since these features are weak and broad and arise from an extended region (Gardner *et al.* 1971 determined a source size of 1.′2 ± 0.′4 for the 4660-MHz emission), they satisfy the criteria for QT emission. The deviations from the optically thin LTE relative intensities (the 4660:4750:4765 ratios are found to be 4:2:1 instead of 1:2:1) may be attributable to disturbance of the hyperfine populations by trapped far-infrared radiation, perhaps a weak form of the disturbance which produces the 4660-MHz maser feature.

An attempt to detect associated QT emission features from the $^2\Pi_{1/2}$, $J = 3/2$ state in Sgr B2 has resulted in upper limits of 0.6 Jy to any features in the $\Delta F = 0$ transitions and 0.3 Jy to any features in the $\Delta F = +1$ transition (Dickinson and Kojoian, private communication).

iii) *W51*

Figures 4 and 5 show the spectra of the $^2\Pi_{3/2}$, $J = 5/2$, $F = 3 \rightarrow 3$ and $F = 2 \rightarrow 2$ transitions. This maser source was originally detected at 6035 MHz by Dr. C. A. Gottlieb, of the Harvard College Observatory, and one of the authors (P. P.) in 1971. W51 is a curious borderline case between class I and class II*a* ground-state maser emission. The velocity of the 5-cm emission is near, but not coincident with, the 1665-MHz and the unusually strong 1720-MHz emission. There are several pairs of 5-cm features with opposite circular polarizations, suggestive of Zeeman doublets. The implied field strengths, shown in Table 8, are similar to those derived for W3(OH) and NGC 6334 N by Zuckerman *et al.* (1972). However, even including magnetic effects, there is no correspondence of ground-state and excited-state features. A number of molecular features, including H_2O maser emission, are found at velocities near the 5-cm emission. There is an associated extended 2.2-μ source, but no discrete infrared sources have been found at the OH position (Wynn-Williams, Becklin, and Neugebauer 1974).

We searched for emission from all three lines of the $^2\Pi_{1/2}$, $J = 1/2$ state, and the limits are given in Table 3. We have not searched either excited state for emission at the velocities corresponding to the ~ 5.8 km s^{-1} ground-state class II*a* features.

iv) *NGC 7538*

Figure 6 displays the linear and circular spectra of the $^2\Pi_{3/2}$, $J = 5/2$, $F = 3 \rightarrow 3$ transition. Maser emission is again found, although without circular polarization. The velocity of the observed feature, -59.7 km s^{-1}, corresponds with that of the single emission feature at 1665 MHz and the unpolarized emission feature at 1720 MHz (cf. Hardebeck 1971). NGC 7538 is similar to W51 in that its ground-state emission has both class I and class II*a* characteristics. Maser emission from H_2O and emission from several millimeter-wavelength molecular lines have been found at velocities near, but not the same as, the 6035-MHz feature. Radio continuum observations (Israel, Habing, and de Jong 1973) show a source of diameter $\leq 0.''5$ at the southern edge of a shell-like H II region. There is a strong 20-μ source at the position of the OH emission (Wynn-Williams *et al.* 1974).

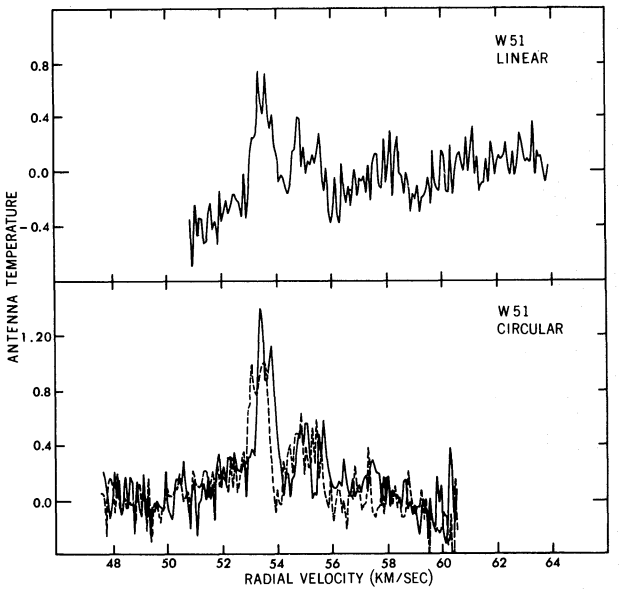

FIG. 4.—The $^2\Pi_{3/2}$, $J = 5/2$, $F = 3 \rightarrow 3$ transition in W51. The frequency resolution is 2 kHz.

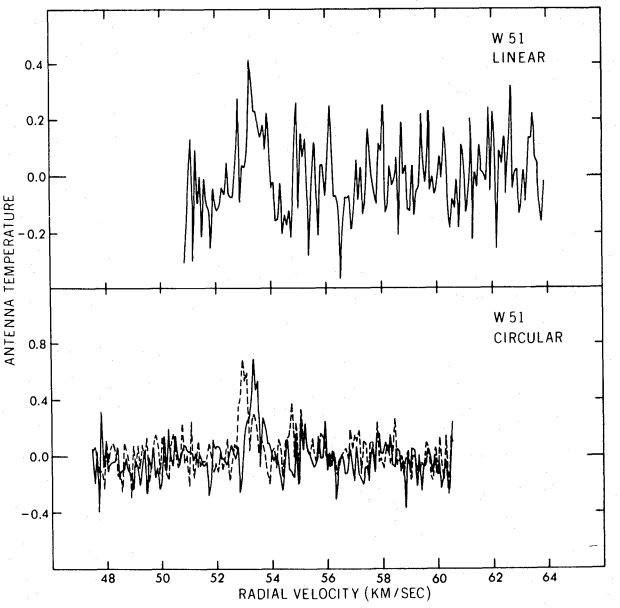

FIG. 5.—The $^2\Pi_{3/2}$, $J = 5/2$, $F = 2 \rightarrow 2$ transition in W51. The frequency resolution is 2 kHz.

TABLE 8

POSSIBLE ZEEMAN PATTERNS

Source	Transition	Features	Center Velocity (km s^{-1})	B* (milligauss)
W51.....	6035	1, 2	53.21	5.7
		3, 4	53.66	4.5
		7, 8	55.48	5.9
	6031	1, 2	53.16	4.1
OH 69.5−1.0.....	6035	1, 2	13.71	3.0
		4, 5	15.08	5.7
	1665	(1, 2)	13.7	2.3
		(4, 5)	15.25	5.7
W49.....	6035	1, 2	10.06	4.5

* The rms error due to the velocity resolution is 0.8 milligauss for the 6035-MHz features and 0.5 milligauss for the 6031-MHz features.

v) *OH 69.5−1.0*

The linear and circular spectra of the $^2\Pi_{3/2}$, $J = 5/2$, $F = 3 \rightarrow 3$ transition are shown in Figure 7. The radial velocities of the observed emission features are in the same velocity range as the ground-state class I emission and the H_2O maser emission. The source of the ground-state emission is coincident with a point source of continuum emission ($\leq 6''$ diameter), in a field which is optically obscured but unusually clear in the radio region (Winnberg, Habing, and Goss 1973). Emission from the $J = 1 \rightarrow 0$ transition of CS has recently been detected in this source (Turner *et al.* 1973).

There are two pairs of features that may be interpreted as Zeeman doublets, and these are presented in Table 8 along with possibly correlated features in the ground-state emission pattern taken from Winnberg (1970). The correspondence with the ground state is considerably better for features 1 and 2 than for features 4 and 5. There does not appear to be any ground-state feature associated with the unpolarized feature 3, nor is there any specific coincidence with the velocity of the H_2O maser feature.

vi) *M17*

M17, one of the strongest thermal radio sources in the Galaxy, is unusual in that its H_2O emission was discovered before its OH emission (Johnston, Sloanaker, and Bologna 1973). There are two H_2O emission features, at $+13.4$ and $+0.6$ km s^{-1}; the 13.4 km s^{-1} feature is known to be variable. The ground-state emission is weak, occurring at $\sim +22$ km s^{-1} (Turner, private communication). The 5-cm emission consists of two features in both the $F = 3 \rightarrow 3$ and $F = 2 \rightarrow 2$ transitions, shown in Figures 8 and 9. There appears to be no correlation with the H_2O emission features, and there is no associated 6-cm emission. Kleinmann and Wright (1973) have discovered a small ($< 10''$), hot (~ 200 K) infrared source near, but apparently not coincident with, the H_2O source.

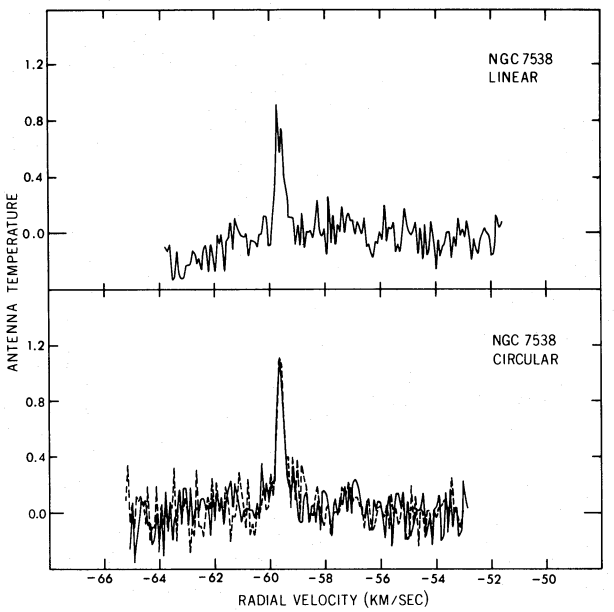

FIG. 6.—The $^2\Pi_{3/2}$, $J = 5/2$, $F = 3 \rightarrow 3$ transition in NGC 7538. The frequency resolution is 2 kHz.

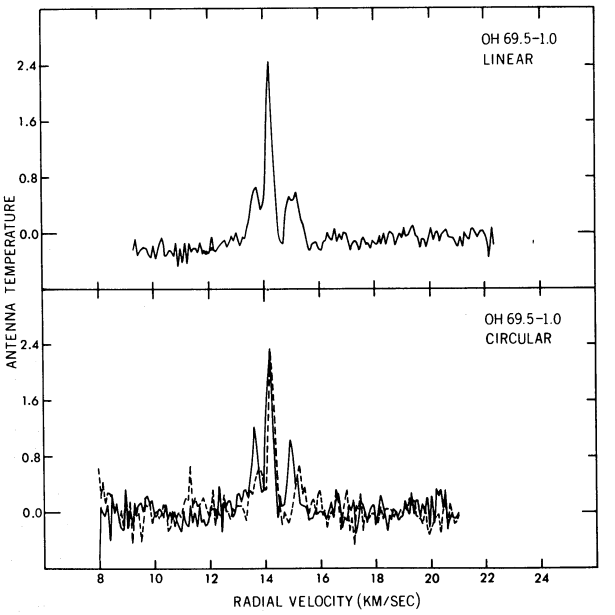

FIG. 7.—The $^2\Pi_{3/2}$, $J = 5/2$, $F = 3 \rightarrow 3$ transition in OH 69.5−1.0. The frequency resolution is 2 kHz.

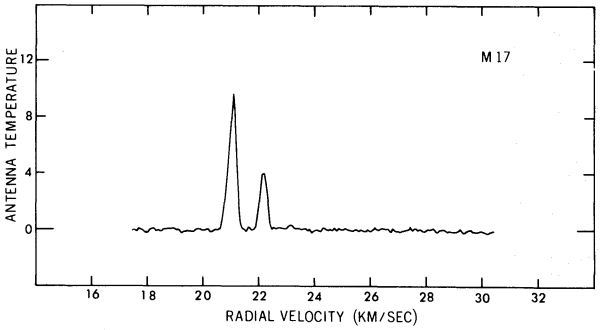

FIG. 8.—The $^2\Pi_{3/2}$, $J = 5/2$, $F = 3 \rightarrow 3$ transition in M17. The frequency resolution is 2 kHz.

vii) *Orion (OH)*

Figure 10 displays the spectrum of the $^2\Pi_{1/2}$, $J = 1/2$, $F = 0 \rightarrow 1$ (4660 MHz) transition. The 8.4 km s^{-1} feature may be matched up with an inconspicuous left circularly polarized feature at 1665 MHz (feature 8 in Palmer and Zuckerman 1967), but there is no obvious ground-state feature associated with the 13.5 km s^{-1} feature. There is, though, maser emission at 1665 and 1612 MHz over the general radial-velocity range of the 6-cm features. Similarly, there is no specific H_2O maser feature associated with either 6-cm feature, but there is H_2O emission over the general radial-velocity range. All other transitions at 5 and 6 cm have been searched in this source, with negative results of comparable sensitivity (cf. Zuckerman *et al.* 1968; Zuckerman and Palmer 1970; this paper, Table 3). At present, Orion is the only 6-cm source which does not display 5-cm emission as well.[4]

c) Time Variations

i) *Sagittarius B2*

Figure 11 displays the spectrum of the $^2\Pi_{3/2}$, $J = 5/2$, $F = 3 \rightarrow 3$ transition as it was recorded on 1972

[4] During recent observations (1974 November), we have detected 5-cm emission features toward Orion (OH). The two principal features are centered at −5.5 and +24 km s^{-1}, and are strong enough to have been easily detectable in previous searches.

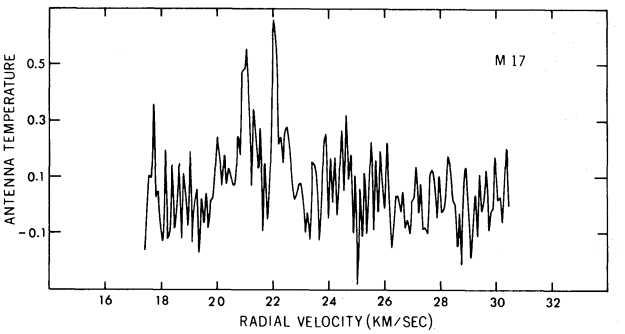

FIG. 9.—The $^2\Pi_{3/2}$, $J = 5/2$, $F = 2 \rightarrow 2$ transition in M17. The frequency resolution is 2 kHz.

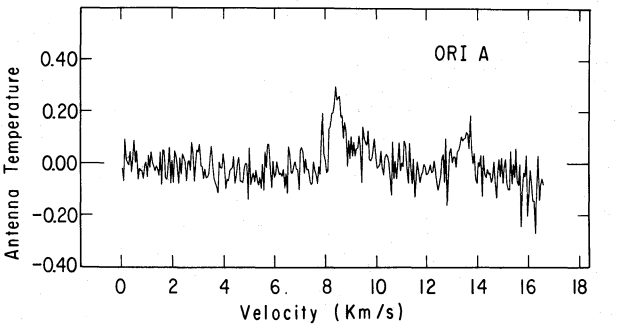

FIG. 10.—The $^2\Pi_{1/2}$, $J = 1/2$, $F = 0 \rightarrow 1$ transition in Orion (OH). The frequency resolution is 1 kHz.

December 1 from 14^h58^m to 18^h53^m LST. The dashed feature indicates the intensity of the 48 km s^{-1} feature as measured the previous day, from 15^h15^m to 17^h13^m LST. Since there were no problems with interference at the time of the measurements, and no interference effects show up in the minute-by-minute records, and since the 48 km s^{-1} feature is present in the average of all spectra (excluding the first day), we interpret this as a probable secular variation. The time scale on which $\Delta T_A/T_A \sim 1$ is ~ 8 hours, slightly shorter than the time scale observed by Zuckerman *et al.* (1972) for a group of features in NGC 6334 N.

We also have evidence for a variation of longer time scale in this source. In our spectra from 1972 March, the ratio of intensities of the 62 and 67 km s^{-1} features was 1/2. In December, this ratio had decreased to $\sim 1/4$. Since, to within the noise of the observations, there was no variation in the intensities of the 67 and 72 km s^{-1} features over this period, this indicates a secular variation in the 62 km s^{-1} feature. The time scale of this variation (9 months) is typical of variations in ground-state OH sources.

ii) *W51*

The appearance of the $^2\Pi_{3/2}$, $J = 5/2$, $F = 3 \rightarrow 3$ spectrum in 1972 March and December and 1973 August is summarized in Table 9. The 1972 observations were made with the same spectral resolution

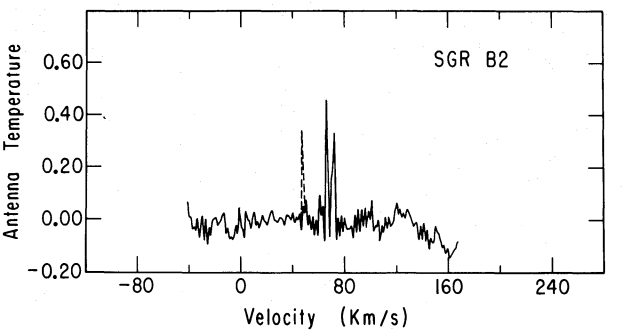

FIG. 11.—The $^2\Pi_{3/2}$, $J = 5/2$, $F = 3 \rightarrow 3$ transition in Sgr B2. The frequency resolution is 31.5 kHz. The solid line is the spectrum as seen on December 1. The dashed feature shows the appearance of the 48 km s^{-1} feature on the previous day.

TABLE 9

TIME VARIATIONS IN W51 AT 6035 MHz

V_{LSR} OF FEATURE (km s^{-1})	T_A (K)		
	1972 March	1972 December	1973 August*
50.5	0.19	< 0.16†	< 0.14†
52	0.30	< 0.16†	< 0.14†
53.3	0.43	< 0.70	0.98
54.5	0.40	0.35‡	0.40
55.7	0.29	< 0.16†	0.25

* Average of equal amounts of left- and right-circular polarization data.

† 3 × rms noise.

‡ Appears to be centered at +55.0 km s^{-1}.

(8 kHz); the August observations were made with 2 kHz resolution, but have been degraded for purposes of comparison. The features at 50.5 and 52 km s^{-1} may be coincident with absorption features seen at 1665 and 1667 MHz, respectively (Goss 1968). Once again, the time scale of the variation is that typical of ground-state OH variations.

iii) *W3(continuum)*

Zuckerman and Palmer (1970) searched the 4765-MHz transition in W3(cont) to an upper limit (peak-to-peak noise) of 0.3 K. However, during our observations of 1973 July—made with the same telescope, the same spectral resolution, and a receiver of similar sensitivity—the −33.9 km s^{-1} feature was present with an antenna temperature of 0.7 K. We infer that at the time of the Zuckerman and Palmer observations (1969 March) the −33.9 km s^{-1} feature was considerably weaker than at present, and perhaps was not present at all. This is the only known case of a variation in a 6-cm OH spectrum.

The 1720-MHz maser source detected by Turner (1970) in 1969 August/September ought to have been within the beam of Weaver, Dieter, and Williams (1968), manifesting itself as a feature of ∼0.5 K antenna temperature at −41 km s^{-1}. There is no feature at that velocity in the Weaver *et al.* spectrum to within a peak-to-peak noise of ∼0.2 K. Thus it seems likely that the 1720-MHz emission also "turned on" recently. We postpone further discussion of these features to § III *b*.

iv) *Other Sources*

In 1972 March, we attempted to reobserve the 5-cm features seen in NML Cygnus by Zuckerman *et al.* (1972). The limits are given in Table 7. NML Cyg is the only infrared star known to have displayed excited-state OH emission. We did not observe any variations in NGC 6334 N; in particular, we did not detect the rapidly variable features observed by Zuckerman *et al.* (1972) in 1970. We also did not see any variations—outside those attributable to the noise—in W75 N. In particular, we find no evidence for the ∼5-month periodicities in the 6.5 km s^{-1} feature proposed by Rydbeck, Kollberg, and Elldér (1970), but also not seen by Zuckerman *et al.* (1972). We also find no evidence for variations in the 5-cm spectra of W3 (OH), W49, NGC 7538, OH 69.5−1.0, and NGC 6334 N (those features not involved in the rapid variation reported by Zuckerman *et al.*) or in the 6-cm spectra of W3 (OH) or Orion (OH).

III. DISCUSSION

a) Quasi-thermal Features

We may derive some of the physical conditions in the W3(cont) source by comparing the 5-cm results with the ground-state observations of Turner (1970); in particular, we will compare the 6035-MHz feature with the corresponding one at 1667 MHz. First, we will express the results in terms of the relative populations of the levels, i.e., the excitation temperatures. Assuming $h\nu/k \ll T_{ex}$ (the excitation temperature) for both transitions, we write the expression for the ratio of the optical depths (τ) at 5 and 18 cm,

$$\frac{\tau_5}{\tau_{18}} = \frac{A_5 \nu_{18} \Delta\nu_{18} n_{l,5} L_5 T_{ex,18}}{A_{18} \nu_5 \Delta\nu_5 n_{l,18} L_{18} T_{ex,5}}$$

Here, A is the spontaneous de-excitation rate, $\Delta\nu$ the Doppler width, and $n_l L$ the projected density of the lower state of a particular transition. With the standard solution of the equation of transfer for the case of small τ, and noting that for this source the brightness temperature of the background continuum (T_B) is likely to be much larger than both $T_{ex,5}$ and $T_{ex,18}$, we obtain

$$\frac{h\nu_{IR}}{kT_{ex,84}} = -\ln\left(\kappa^2 \frac{g_{l,18} A_{18} \nu_5 \Delta\nu_5 T_{A,5} D_{18} T_{B,5} T_{ex,5}}{g_{l,5} A_5 \nu_{18} \Delta\nu_{18} T_{A,18} D_5 T_{B,5} T_{ex,18}}\right). \quad (1)$$

Here, we related the populations of the lower levels of the 18-cm and 5-cm doublets by $n_{l,5}/n_{l,18} = (g_{l,5}/g_{l,18}) \exp(-h\nu_{IR}/kT_{ex,84})$. We also set $L_{18} = \kappa L_5$ and assumed that the 18-cm absorption is uniform, so that we may separate out that part arising from the region of the 5-cm absorption. T_A is the antenna temperature for a particular transition, and D is the appropriate beam dilution factor, ranging from $\eta_A(\Omega_S/\Omega_B)$, for a source much smaller than the beam, to η_B, for a source filling the beam (η_A and η_B are the

aperture and beam efficiency, and Ω_S and Ω_B are the solid angles subtended by the source and by the antenna beam).

We can then solve equation (1) for $T_{\mathrm{ex},84}$ as a function of κ and $\mu \equiv T_{\mathrm{ex},5}/T_{\mathrm{ex},18}$. However, the W3(cont) region is fairly complex, and we know neither the size of the OH cloud nor what component of the background continuum it is absorbing. Examination of the fluxes and sizes of components A, B, and D of the radio continuum source (Wynn-Williams 1971) shows that neither component B nor component D alone is strong enough to account for the flux absorbed out in the line. Thus, either component A alone or a combination of the three provides the flux being absorbed. (The mapping results are consistent with either case.) First, we assume that the cloud lies entirely in front of component A, and we take the angular size of the OH cloud to be equal to that of component A. (Beam-filling arguments show that the cloud cannot be much smaller [the lower limit is $\sim 0'.2$], and any part of the cloud lying beyond the extent of component A would not contribute to the observed absorption feature.)

For the solution of equation (1), we take $A_5 = 1.55 \times 10^{-9}\ \mathrm{s}^{-1}$, $A_{18} = 7.71 \times 10^{-11}\ \mathrm{s}^{-1}$, $\Delta\nu_5 = 88.6$ kHz, $\Delta\nu_{18} = 26$ kHz, $T_{A,5} = -0.15$ K, $T_{A,18} = -2.7$ K, $\eta_{A,5} = 0.49$, and $\eta_{A,18} = 0.53$. For component A, we use $T_{B,18} = 8.40 \times 10^3$ K, $T_{B,5} = 1.02 \times 10^3$ K, and $\Omega_S = 2.91 \times 10^{-8}$ sr. We obtain $\tau_5 = 1.78 \times 10^{-2}$, $\tau_{18} = 0.45$, and

$$T_{\mathrm{ex},84} = 121/(4.05 - \ln \mu\kappa^2)\,.$$

(Note that the relative intensities of the 18cm lines [Turner 1970] are consistent with the above result of low optical depth at 1667 MHz.) Setting $\mu = 1$ and $\kappa = 1$ yields $T_{\mathrm{ex},84} = 29.9$ K. We may then solve for the infrared optical depth. Since the lower levels of the 18-cm and the infrared transitions are the same, we assume that both transitions are characterized by the same velocity widths, and derive

$$\tau_{84} = (4.08 - 7.10 \times 10^{-2}\mu\kappa^2)T_{\mathrm{ex},18}/\kappa\,.$$

For $\mu = 1$ and $\kappa = 1$, this implies $\tau_{84} = 4T_{\mathrm{ex},18}$. In this case, then, for the range of excitation temperatures expected, the infrared radiation will be important in populating the excited rotational state.

In order to relate the ground-state and excited-state populations and to find the excitation temperatures, it is necessary to solve the equations of statistical equilibrium. At present, the collision cross sections are not well enough known to enable accurate calculations of the Λ-doublet excitation temperatures. Simply equating the collisional excitation and spontaneous radiative decay rates suggests that high densities are required. However, taking into account radiative excitation by the far-infrared continuum of W3, we find that high densities need not necessarily be invoked. In fact, we demonstrate (1) that, for appropriate location of the OH cloud, direct infrared excitation can explain the population of the $J = 5/2$ state, and (2) that if this geometric condition is not satisfied, rather large densities are required (even when trapping of the 84 cm^{-1} radiation is included).

We write the equation of statistical equilibrium for these two rotational levels:

$$\frac{n_{\mathrm{H}_2}\langle\sigma v\rangle}{A_{84}'}\left[\exp\left(-\frac{h\nu_{84}}{kT_{\mathrm{ex},84}}\right) - \exp\left(-\frac{h\nu_{84}}{kT_K}\right)\right] = \mathscr{I}\left[1 - \exp\left(-\frac{h\nu_{84}}{kT_{\mathrm{ex},84}}\right)\right] - \exp\left(-\frac{h\nu_{84}}{kT_{\mathrm{ex},84}}\right)\cdot \quad (2)$$

Here, $n_{\mathrm{H}_2}\langle\sigma v\rangle$ is the collisional de-excitation rate, T_K is the kinetic temperature of the collisional environment, $\mathscr{I}$ is the photon occupation number for photons of energy $h\nu_{84}$, and A_{84}' is the spontaneous radiative de-excitation rate corrected for the effects of trapped infrared radiation (cf. Sobolev 1963):

$$A_{84}' = \frac{A_{84}}{\tau_{84}(\pi \ln \tau_{84})^{1/2}} \quad (\text{for } \tau_{84} > 10)\,.$$

W3 is a strong far-infrared source, which can be considered at these wavelengths as a 77 K blackbody (Harper 1974), and is the dominant contributor to $\mathscr{I}$. If we write $\mathscr{I} = [\exp(h\nu_{84}/kT_R) - 1]^{-1}$, then T_R is the temperature of an isotropic blackbody radiation field that would provide the same energy density at ν_{84} as that provided by the background source.

The infrared excitation temperature is determined from the observations, after a choice of μ and κ. The expected range of $T_{\mathrm{ex},84}$, as a function of n_{H_2} and T_K, may be computed from equation (2) after a choice of $\tilde{\Omega}_S$, the solid angle subtended by the far-infrared source at the OH cloud. Thus, according to the distance of the cloud from the continuum source, the observed $T_{\mathrm{ex},84}$ may be close to T_R, or it may be much different from T_R. (This distinction is of interest because, when $T_{\mathrm{ex},84} \approx T_R$, it is no longer necessary to solve eq. [2].) For $T_{\mathrm{ex},84} \approx T_R$, this distance must be such that

$$\frac{4\pi}{\tilde{\Omega}_S} = \frac{15.05}{\mu\kappa^2} - 0.262\,. \quad (3)$$

For $\mu\kappa^2 = 1$, $\tilde{\Omega}_S/4\pi \approx 0.07$. In principle, $\tilde{\Omega}_S/4\pi$ could range from $\sim 1/2$, if the OH cloud is very near the far-infrared source, to ~ 0.01, if the cloud is in the outer regions of the W3 complex.

In the case that $T_{\mathrm{ex},84} \approx T_R$, the excitation is due almost entirely to radiative excitation by the far-infrared source. In fact, setting $T_R = T_{\mathrm{ex},84}$ in equation (2) will make the right-hand side vanish, indicating a solution for all values of n_{H_2} if $T_K = T_R$ and no solution otherwise. Such a solution is not necessary, though; it is only required that for such positions of the OH cloud for which the right-hand side becomes small, there is a range of values of n_{H_2} and T_K for which the left-hand side becomes equally small. This range decreases as the distance between cloud and infrared source increases (because of the dependence of this case on the efficacy of radiative excitation). But for reasonable values of n_{H_2}, T_K, μ, and κ, the present observations can be explained by direct far-infrared

excitation. Of course, supporting evidence (such as a measurement of the distance of the OH cloud from the continuum source) is required.

If equation (3) is not satisfied, we must consider the effects of collisions and trapping explicitly. Specifically, we must solve equation (2) for n_{H_2}, a function of T_K, $\langle\sigma v\rangle$, κ, μ, $T_{ex,18}$, and $\tilde{\Omega}_S$. We may simplify the problem somewhat by assuming $T_{ex,18} = T_K$. Furthermore, since $h\nu_{84}/k \gg$ likely values of T_K, we can approximate $\langle\sigma v\rangle$ as a constant (10^{-15} cm^2) times the rms velocity of the H_2 molecules times the fraction of H_2 molecules with energies $h\nu_{84}$, assuming a Maxwellian velocity distribution with temperature T_K. Finally, we have the constraint that either $T_R \leq T_{ex,84} \leq T_K$ or $T_K \leq T_{ex,84} \leq T_R$. There is still a wide range in the possible parameter values that will satisfy equation (2), and only comparison of the results with other observations will enable the most appropriate selection. Inspection of the case $\mathscr{I} \to 0$ suggests that $n_{H_2} \gtrsim A_{84}'/\langle\sigma v\rangle$, i.e., $n_{H_2} \gtrsim 10^6$–10^7 cm^{-3}. Of course, the effect of the strong far-infrared background will be to reduce the required densities.

We have solved equation (2) for n_{H_2}, choosing several reasonable values for κ, μ, $\tilde{\Omega}_S/4\pi$, and T_K. These are given in Table 10. We also include solutions for the case of pure radiative excitation, distinguished by blank entries for T_K and also indicated by the footnote. Furthermore, we note that Wynn-Williams, Becklin, and Neugebauer (1972) have determined the visual extinction to component A to be 14 ± 3 mag, with about 1 mag of this extinction due to dust mixed with the ionized gas. Taking $A_V = 13$ mag and assuming a typical gas-to-dust ratio

$$(N_{H_2} = 2.2 \times 10^{21} A_V \text{ cm}^{-2} \text{ mag}^{-1}),$$

we obtain $N_{H_2} = 2.9 \times 10^{22}$ cm^{-2} in front of component A. We may use this to relate the calculated n_{H_2} to the thickness, L_5, of the 5-cm absorption region: L_5(pc) $= 9.3 \times 10^3/n_{H_2}$(cm^{-3}). (The pure radiative solutions are independent of density, but we can estimate n_{H_2} by assuming a value for L_5 [taking a spherical cloud of the proper angular size] and using the above N_{H_2}. These values are also given in Table 10, set off by parentheses.) Finally, using the assumed values of κ, μ, and $T_{ex,18}(=T_K)$, we can determine column densities in the 5-cm absorption region. Assuming that the hyperfine levels within each parity state of the Λ-doublets are populated according to their statistical weights, we derive the total column densities in the $J = 5/2$ states and thus obtain N_{OH}, a lower limit to the total OH column density.

For the cases of pure radiative excitation, the derived values of T_K range from 20.3 K to 56.3 K. For the other solutions, the thickness of the OH cloud is severely restricted by the constraint on the associated extinction. However, acceptable solutions can be found for $T_K \sim 100$ K. For $\tilde{\Omega}_S/4\pi = 0.01$, a cloud with $\mu = \kappa = 1$ would be roughly spherical and of size comparable to that of component A (and thus consistent with our earlier assumption about the angular size). For $\tilde{\Omega}_S/4\pi = 0.5$, the deduced densities are fairly high. This is essentially because the strong infrared flux will tend to heat the OH to above the kinetic temperature, and high densities are required for collisions to counteract this effect. For $\mu = \kappa = 2$, the cloud would seem to be a thin shell covering the continuum source, and perhaps surrounding it. The ratio of the thickness of the shell to the radius of component A would be (1–2) × 10^{-2}. For $\tilde{\Omega}_S/4\pi = 0.1$, a fairly large cloud can be obtained at the expense of very large infrared optical depths (~400).

The derived values of N_{OH} are all very similar. We note that, if the H_2 and OH are coexistent and uniformly distributed, then $\kappa N_{OH}/N_{H_2}$ will be a lower

TABLE 10

SELECTED SOLUTIONS FOR W3(Continuum)

κ	μ	$T_{ex,84}$ (K)	$\tilde{\Omega}_S/4\pi$	T_K (K)	n_{H_2} (cm^{-3})	L_5 (pc)	N_{OH} (cm^{-2})
1.....	0.15	20.3	0.01	*	(3.1 × 10^4)	(3 × 10^{-1})	1.0 × 10^{16}
1.....	1	29.9	0.5	25	4.0 × 10^9	2 × 10^{-6}	1.3 × 10^{16}
			0.1	25	3.0 × 10^8	3 × 10^{-5}	1.3 × 10^{16}
			0.07	*	(3.1 × 10^4)	(3 × 10^{-1})	1.5 × 10^{16}
			0.01	50	2.6 × 10^6	4 × 10^{-3}	2.6 × 10^{16}
			0.01	100	8.3 × 10^4	1 × 10^{-1}	5.2 × 10^{16}
1.....	2	36.1	0.5	25	9.7 × 10^8	1 × 10^{-5}	1.3 × 10^{16}
			0.14	*	(3.1 × 10^4)	(3 × 10^{-1})	1.9 × 10^{16}
			0.1	50	2.5 × 10^6	4 × 10^{-3}	2.6 × 10^{16}
			0.1	100	5.8 × 10^4	2 × 10^{-1}	5.3 × 10^{16}
			0.01	50	8.4 × 10^6	1 × 10^{-3}	2.6 × 10^{16}
			0.01	100	1.9 × 10^5	5 × 10^{-2}	5.3 × 10^{16}
1.8.....	2	56.3	0.5	*	(1.7 × 10^4)	(3 × 10^{-1})	1.7 × 10^{16}
2.....	2	61.4	0.5	75	3.9 × 10^6	1 × 10^{-3}	2.1 × 10^{16}
			0.5	100	6.5 × 10^5	7 × 10^{-3}	2.8 × 10^{16}
			0.1	75	1.7 × 10^7	3 × 10^{-4}	2.1 × 10^{16}
			0.1	100	2.9 × 10^6	2 × 10^{-3}	2.8 × 10^{16}
			0.01	75	2.0 × 10^7	2 × 10^{-4}	2.1 × 10^{16}
			0.01	100	3.4 × 10^6	1 × 10^{-3}	2.6 × 10^{16}

* Pure radiative excitation. Because there is a range of possible values, no entry is given for T_K. Values for n_{H_2} are derived from an assumed value for L_5.

limit to the abundance ratio [OH]/[H_2] in the 5-cm absorption region. The values range from 3.4×10^{-7} to 1.9×10^{-6}.

In the case that the OH cloud lies in front of all three continuum sources, the results are similar to those given above, pointing out the relative weakness of components B and D. We obtain $\tau_5 = 1.34 \times 10^{-2}$, $\tau_{18} = 0.358$, $T_{ex,84} = 121/(4.11 - \ln \mu\kappa^2)$, and $\tau_{84} = (4.08 - 6.70 \times 10^{-2}\mu\kappa^2)T_{ex,18}/\kappa$. For radiative excitation, $T_K = T_{ex,84}$ ranges from 56.0 K (for $\tilde{\Omega}_S/4\pi = 0.5$) to 20.4 K (for $\tilde{\Omega}_S/4\pi = 0.01$). For collisional excitation, the results are also similar to those in Table 10, with n_{H_2} typically $\sim 10^6$ cm^{-3} at $T_K = 50$ K.

We also mention the possibility that the excitation temperatures of the 18-cm and 5-cm transitions are anomalously lowered below 2.7 K, so that the OH is seen absorbing the microwave background radiation (in the same manner as the anomalous 6-cm formaldehyde absorption features seen in dark clouds). In this case, beam-filling arguments require the source to have an angular size larger than 2′. Thus, the cloud would have to be behind the discrete continuum sources, or it would fall in front of at least one component. A similar condition must hold if the OH cloud is absorbing radiation from the diffuse H II component (seen more prominently at lower frequencies [Wynn-Williams 1971]). In this case, we must additionally stipulate that the discrete continuum sources lie in front of the diffuse H II region. For an OH cloud of diameter $\gtrsim 2'$, the mass will be $\gtrsim 1.4 n_{H_2} M_\odot$. Even for densities rather less than those required to provide sufficient population of the 5-cm doublet, this mass will be quite large, suggesting that these models are unlikely to be correct.

Finally, we note that, if, in the case of pure radiative excitation, the $^2\Pi_{1/2}, J = \frac{1}{2}$ state is also directly excited by the background radiation source, we may relate our upper limit for 6-cm absorption to the ratio of the 6-cm and 5-cm excitation temperatures. If the path lengths are equal for both states, the source smaller than the beam at both wavelengths, and the excitation temperatures small compared with the background temperature, and if the background continuum source is optically thin, then the negative result at 6 cm implies $T_{ex,6} > T_{ex,5}$. If, however, both states are populated by collisions, so that the lower $^2\Pi_{1/2}, J = \frac{1}{2}$ population is due to the Boltzmann factor, then we may infer $T_K < 165$ K.

In the case of Sgr B2, we may suppose that we are seeing an object similar to the W3 cloud, but which does not happen to lie in front of a strong continuum source (or else $T_{ex,6}$ and $T_{ex,5}$ are negative). As discussed above, the densities required are fairly large—even when far-infrared trapping is included—and this suggests that the QT excited OH features arise from the dense core seen in some millimeter-wavelength molecular studies (Solomon *et al.* 1971; Morris *et al.* 1973), which has a density $\gtrsim 10^6$ cm^{-3}. Unfortunately, the analysis is not as straightforward as that for W3, principally because of the lack of any particular ground-state feature that can be associated with the excited-state features.

If the excited states are populated according to thermodynamic equilibrium at the kinetic temperature of the gas, then the ratio of the brightness temperatures of the 4750-MHz and 6031-MHz features would be $0.29 \exp(-61.3/T_K)$. The observed ratio is 2.5, requiring us to find ways to increase the population in the $^2\Pi_{1/2}, J = \frac{1}{2}$ state, or perturb the excitation temperatures at 6 and 5 cm. One way of surmounting the Boltzmann factor would be to put the OH in a dilute, hot ($T_K \gg 100$ K) gas that would collisionally excite much higher rotational levels. Depopulation of the excited states would then proceed by radiative decay. If the infrared transitions are optically thin and the cross sections for excitation into the $^2\Pi_{3/2}$ and $^2\Pi_{1/2}$ ladders are equal, then the relative populations of the 5-cm and the 6-cm doublets will be determined by the ratio of the Einstein A's of the infrared transitions. The resulting ratio of the brightness temperatures of the 4750-MHz and 6031-MHz features is ~ 3.5, if the hyperfine levels are populated according to their statistical weights. However, it is difficult to understand why this hot gas is not seen in other observations of the dense core (e.g., Solomon *et al.* 1973).

Furthermore, if we assume that $\tau \ll 1$ and $h\nu/kT_{ex} \ll 1$ for the 4750-MHz feature, we derive a minimum column density of $\sim 2 \times 10^{16}$ cm^{-2} for the $^2\Pi_{1/2}, J = \frac{1}{2}$ state. The ground-state column density would be at least equal to this figure, and would imply optical depths $\gg 1$ for the infrared transitions. Because of the larger Einstein A for the 84 cm^{-1} transitions, trapping of far-infrared radiation would result in an undesired enhancement of the population of the $^2\Pi_{3/2}, J = 5/2$ state. It may be that the cross-sections for collisional excitation are unequal, but, because of the spin change involved in excitation into the $^2\Pi_{1/2}$ ladder, such an inequality would be expected to favor further enhancement of the $^2\Pi_{3/2}, J = 5/2$ population.

It thus appears that the observed ratio of brightness temperatures cannot be accounted for by a difference in population of the excited states. A possible alternative explanation would be a difference in the doublet excitation temperatures. We have done a statistical equilibrium calculation for the three doublets, neglecting hyperfine structure and approximating the effects of radiative transfer in the infrared lines by the use of trapping factors (Litvak 1972). Although the calculation was of insufficient sophistication to reproduce the observations, it commonly showed enhancement of the 6-cm excitation temperature. Another alternative would be to assume that the 6-cm emission occurs over a larger region than the 5-cm emission. To reproduce the observed brightness temperature ratio, we must require that the diameter of the 5-cm region be less than half of the 6-cm region. The present observations do not allow a decision between these possibilities.

Finally, we note that we may use the QT features to obtain upper limits to the magnetic field strengths in the Sgr B2 and W3(cont) molecular clouds. The 5-cm and 6-cm line widths in Sgr B2 are approximately equal, and thus the magnetic field strength must be $\lesssim 0.2$ gauss (otherwise, Zeeman effects would make the 5-cm lines much broader than the 6-cm lines). In

W3(cont), the widths of the 5-cm absorption features suggest field strengths $\lesssim 0.05$ gauss. These fields are much weaker than those suggested for the dense molecular region in Orion by Clark and Johnson (1974).

b) *Maser Features*

Zuckerman *et al.* (1968) suggested that, in regions where the hyperfine levels of the ground state are populated such that the 1612-MHz transition is in maser emission, trapping of 126 cm^{-1} radiation should result in emission at 4660 MHz. Thus, there are many strong maser features in the 1612-MHz spectrum of Orion, and the detection of this source at 4660 MHz suggests appreciable far-infrared trapping. Far-infrared trapping should also result in a correlation of 1720-MHz and 4765-MHz maser emission—the observational support for this correlation has been discussed by Thacker, Wilson, and Barrett (1970)—and so it is tempting to speculate that the 1720-MHz and 4765-MHz features in W3(cont) turned on at the same time. This would then limit that time to the 6-month period between the observations of Zuckerman and Palmer (1970) and those of Turner (1970).

We note that (except for NML Cyg) all 5-cm maser sources are associated with class I OH/H_2O sources, and that it thus seems that class I ground-state OH emission, 5-cm emission, and H_2O emission have in common some general mechanism or physical condition leading to inversion. We cannot, however, suggest a detailed correspondence between the emitters. Indeed, Zuckerman *et al.* (1972) have pointed out that there is no evidence for correlation of the Doppler velocities of features at 18, 5, and 1.35 cm, and have suggested that there may even be an anticorrelation. Of the new 5-cm sources reported in this paper, only NGC 7538 shows a correlation with 18-cm features, and this single case may be due to chance. Finally, there does not appear to be any correlation among the intensities of the various sources at 18, 5, and 1.35 cm.

Chemical, near-infrared, and ultraviolet pumping models involve cascades down the ladder of rotational energy levels, producing inversions in excited-state and ground-state Λ-doublets in the same region. Thus there must be some mechanism which obscures the expected correlation of features at 5 and 18 cm. Collisions may destroy the 18-cm inversion at densities where the 5-cm inversion persists; but, since the $J = 5/2$ doublet is populated and inverted by the same cascade process that inverts the 18-cm doublet, it is difficult to understand why almost no 5-cm emission occurs from lower density regions where the 18-cm inversion persists. In this context, the far-infrared pumping mechanism is easier to understand, as the $J = 5/2$ doublet is populated by collisional excitation out of the $J = 3/2$ doublet, and thus when the densities are low enough for 18-cm inversion, there may be insufficient population of the excited state to produce an observable signal. Certainly, interferometer positions for the 5-cm emission features, sufficiently accurate for comparison with 18-cm positions, will be useful. Furthermore, we note that the Zeeman effect will affect the velocity correlation of 5-cm and 18-cm features. While the relative Zeeman shifts are predictable, the distortion of the ground-state Zeeman patterns could easily obscure any connections with excited-state features.

The rapid time variation observed in Sgr B2 suggests a maximum size to the amplifying region of ~ 60 AU if the feature was well saturated. The maximum size may be increased by a factor G (where G is the gain of the amplifying region) if the feature was unsaturated. (Typical values for G are 15 to 20.) Zuckerman *et al.* (1972) have pointed out, with regard to the rapid variation in NGC 6334 N, that the latter case is more plausible. Yet, if we apply the formulae of Goldreich and Keeley (1972), using parameters appropriate to the $^2\Pi_{3/2}$, $J = 5/2$ state ($A = 1.55 \times 10^{-9}$ s^{-1}, $\Delta v = 0.5$ km s^{-1}, fractional pump rate $\Delta R/R = 10^{-2}$, decay rate $\Gamma = 0.137$ s^{-1}) and assuming that the total population in the $^2\Pi_{3/2}$, $J = 5/2$ state is roughly one-third of the total OH density (i.e., like a Boltzmann distribution with $T_K = 100$ K), we find that a 600 AU cloud would be overwhelmingly saturated. In fact, a 60 AU maser would be completely saturated, and so represents a definite upper limit to the source size. The apparent size of such a maser would be less than 2 AU, well below the upper limits of 50 AU determined by interferometric observations (Knowles *et al.* 1973).

We wish to thank Mr. Craig Moore, Mr. Charles Brockway, and Mr. Thomas Dunbrack for their help with the equipment, and Drs. David Buhl and Stuart Mufson for their assistance with one phase of the data reduction. We also thank Dr. Barry Turner and Mr. Mark Morris for some enlightening discussions. Partial financial support for this work came from NSF grants 24779-A2 to the University of Chicago and GP-26218 to the University of Maryland, and from the Alfred P. Sloan Foundation.

REFERENCES

Clark, F. O., and Johnson, D. R. 1974, *Ap. J.* (*Letters*), **191**, L87.
Gardner, F. F., and Ribes, J. C. 1971, *Ap. Letters*, **9**, 175.
Gardner, F. F., Ribes, J. C., and Sinclair, M. W. 1971, *Ap. J.* (*Letters*), **169**, L109.
Goldreich, P., and Keeley, D. A. 1972, *Ap. J.*, **174**, 517.
Goss, W. M. 1968, *Ap. J. Suppl.*, **15**, 131.
Hardebeck, E. 1971, *Ap. J.*, **170**, 281.
———. 1972, *ibid.*, **172**, 583.
Harper, D. A. 1974, *Ap. J.*, **192**, 557.
Israel, F. P., Habing, H. J., and de Jong, T. 1973, *Astr. and Ap.*, **27**, 143.
Johnston, K. J., Sloanaker, R. M., and Bologna, J. M. 1973, *Ap. J.*, **182**, 67.
Kleinmann, D. E., and Wright, E. L. 1973, *Ap. J.* (*Letters*), **185**, L131.
Knowles, S. H., Johnston, K. J., Moran, J. M., and Ball, J. A. 1973, *Ap. J.* (*Letters*), **180**, L117.
Litvak, M. M. 1972, *Atoms and Molecules in Astrophysics*, ed. T. R. Carson and M. J. Roberts (London: Academic Press), p. 201.
Morris, M., Palmer, P., Turner, B. E., and Zuckerman, B. 1973, *Interstellar Dust and Related Topics, IAU Symposium No. 52*, ed. J. M. Greenberg and H. C. van de Hulst (Dordrecht: Reidel), p. 485.
Palmer, P., and Zuckerman, B. 1967, *Ap. J.*, **148**, 727.
Rickard, L. J Zuckerman, B., and Palmer, P. 1972, *Bull. AAS*, **4**, 307.

Rickard, L. J, Zuckerman, B., and Palmer, P. 1973, *Bull. AAS*, **5**, 331.
Rydbeck, O. E. H., Kollberg, E., and Elldér, J. 1970, *Ap. J. (Letters)*, **161**, L25.
Sobolev, V. V. 1963, *Treatise on Radiative Transfer* (Princeton: van Nostrand).
Solomon, P. M., Jefferts, K. B., Penzias, A. A., and Wilson, R. W. 1971, *Ap. J. (Letters)*, **168**, L107.
Solomon, P. M., Penzias, A. A., Jefferts, K. B., and Wilson, R. W. 1973, *Ap. J. (Letters)*, **185**, L63.
Sullivan, W. T., III. 1971, *Ap. J.*, **166**, 321.
Thacker, D. L., Wilson, W. J., and Barrett, A. J. 1970, *Ap. J. (Letters)*, **161**, L191.
Turner, B. E. 1970, *Ap. Letters*, **6**, 99.
Turner, B. E., Palmer, P., and Zuckerman, B. 1970, *Ap. J. (Letters)*, **160**, L125.
Turner, B. E., Zuckerman, B., Palmer, P., and Morris, M. 1973, *Ap. J.*, **186**, 123.
Weaver, H., Dieter, N. H., and Williams, D. R. W. 1968, *Ap. J. Suppl.*, **16**, 219.
Winnberg, A. 1970, *Astr. and Ap.*, **9**, 259.
Winnberg, A., Habing, H. J., and Goss, W. M. 1973, *Nature Phys. Sci.*, **243**, 78.
Wynn-Williams, C. G. 1971, *M.N.R.A.S.*, **151**, 397.
Wynn-Williams, C. G., Becklin, E. E., and Neugebauer, G. 1972, *M.N.R.A.S.*, **160**, 1.
———. 1974, *Ap. J.*, **187**, 473.
Yen, J. L., Zuckerman, B., Palmer, P., and Penfield, H. 1969, *Ap. J. (Letters)*, **156**, L27.
Zuckerman, B., and Palmer, P. 1970, *Ap. J. (Letters)*, **159**, L197.
Zuckerman, B., Palmer, P., Penfield, H., and Lilley, A. E. 1968, *Ap. J. (Letters)*, **153**, L69.
Zuckerman, B., Yen, J. L., Gottlieb, C., and Palmer, P. 1972, *Ap. J.*, **177**, 59.

LEE J RICKARD and PATRICK PALMER: Department of Astronomy and Astrophysics, University of Chicago, 1100–14 E. 58th St., Chicago, IL 60637

BEN ZUCKERMAN: Astronomy Program, University of Maryland, College Park, MD 20742